Journal of Nuclear Materials 389 (2009) 317–325

Contents lists available at ScienceDirect

Journal of Nuclear Materials

journal homepage: www.elsevier.com/locate/jnucmat

Proton irradiation study of GFR candidate ceramics

Jian Gan [a,*], Yong Yang [b], Clayton Dickson [b], Todd Allen [b]

[a] Idaho National Laboratory, Idaho Falls, Idaho, USA
[b] University of Wisconsin, Madison, Wisconsin, USA

A B S T R A C T

This work investigated the microstructural response of SiC, ZrC and ZrN irradiated with 2.6 MeV protons at 800 °C to a fluence of 2.75×10^{19} protons/cm^2, corresponding to 0.71–1.8 displacement per atom (dpa), depending on the material. The change of lattice constant evaluated using HOLZ patterns is not observed. In comparison to Kr ion irradiation at 800 °C to 10 dpa from the previous studies, the proton irradiated ZrC and ZrN at 1.8 dpa show less irradiation damage to the lattice structure. The proton irradiated ZrC exhibits faulted loops which are not observed in the Kr ion irradiated sample. ZrN shows the least microstructural change from proton irradiation. The microstructure of 6H-SiC irradiated to 0.71 dpa consists of black dot defects at high density.

Published by Elsevier B.V.

1. Introduction

Refractory ceramics have been considered for the gas cooled fast reactor (GFR) for their high temperature stability at 1000 °C under normal operation and up to 1600 °C during a loss of coolant accident. Refractory ceramics of ZrC, ZrN and SiC are candidates for both structural and fuel matrix materials due to their neutronic performance, thermal properties, chemical behavior, crystal structure, and physical properties. These transition metal carbides and nitrides have a NaCl type structure. The 6H-SiC is a common form of SiC that has a hexagonal structure. The high dose radiation effects on the microstructure of these ceramics have been studied previously using Kr ion irradiation at 800 °C. Proton irradiation of these ceramics has not been investigated before. It is believed that by using both heavy ion and proton irradiation at relevant conditions, the microstructural response under neutron irradiation in a GFR environment can be anticipated.

Data for high temperature irradiation effects in these materials are sparse. Dyslin et al. reported their work on irradiation studies of refractory materials [1]. When irradiated in the engineering test reactor (ETR) at 130–355 °C up to ~5.2×10^{21} n/cm^2 ($E > 1$ MeV), a volume increase of roughly 2–2.5% and 2–3.3% was observed in TiC and ZrC, respectively. The peak volume increases at these temperatures were around fast neutron fluence of 2.1×10^{21} n/cm^2. The same materials irradiated at 1000–1100 °C to ~3×10^{21} n/cm^2 ($E > 1$ MeV) showed a reduced volume increase with ~0.5% and 1% for TiC and ZrC, respectively. Post-irradiation thermal annealing (700–1100 °C) of TiC and ZrC (irradiated at ~130 °C to ~1.3×10^{21} n/cm^2 for $E > 1$ MeV) indicated a greater shrinkage effect in TiC than in ZrC, suggesting a larger fraction of single defects in TiC. It is believed that single defects are relatively easier to be annealed out.

SiC is a special material due to its electronic properties, thermal stability, extreme hardness, and chemical inertness. The work by Weber et al. [2], on a single crystal 6H-SiC irradiated in-situ along the [0001] orientation with 1.5 MeV Xe ions at temperatures between −253 and 202 °C, revealed that there is a critical temperature of 212 °C above which amorphization does not occur. Persson et al. [3], reported the work on 4H-SiC implanted with 180 keV Al ions at 600 °C to fluences of 1.3 to 7.8×10^{14} ions/cm^2. They found loops at fluences above 2.6×10^{14} ions/cm^2 and these loops reside on the (0001) basal plan with average size of approximately 50 nm. They also reported that the loops in 4H-SiC consist of C, or Si self-interstitials, or both [4].

The previous work on Kr ion irradiation of the GFR candidate ceramics reveals that 6H-SiC has the most stable microstructure among the five materials (ZrC, ZrN, TiC, TiN, and SiC), although dislocation loops are present at 70 displacement per atom (dpa) [5]. TiC and TiN perform better than ZrC and ZrN. Perfect loops are found in both TiC and TiN, but not in ZrC and ZrN. Voids were not found in any of the five ceramics, even at 70 dpa. At an irradiation temperature of 800 °C, no radiation induced amorphization was found up to 70 dpa. While ring patterns were observed in ZrC, an ordered face-centered-cubic (fcc) (Ll_2) structure was identified in ZrN at 70 dpa. The lattice expansion due to irradiation in TiC or TiN is approximately a factor of four lower than in ZrC or ZrN. The absolute values of lattice constant, measured using select area diffraction patterns at major zones, are not reliable even using a nanocrystal Au foil for calibration. However, a more accurate measurement using higher order Laue zone (HOLZ) patterns is not applicable for those high dose irradiated samples.

* Corresponding author.
E-mail address: Jian.Gan@inl.gov (J. Gan).

0022-3115/$ - see front matter Published by Elsevier B.V.
doi:10.1016/j.jnucmat.2009.02.021

This work is to investigate the microstructural response of ZrC, ZrN and SiC irradiated with 2.6 MeV protons at 800 °C. Proton irradiation at this energy will produce a uniformly damaged layer with depth over 30 μm. It has advantage over the Kr ion irradiation where the effective sample depth is less than ~200 nm. Surface oxidation in Kr irradiation created severe problems on the transmission electron microscopy (TEM) analysis of the irradiated samples. For proton irradiated ceramics, a TEM sample can be prepared from the middle section of the damaged layer with a fresh and clean surface on both sides, completely eliminating the surface oxidation problem. This is important to reduce the complexity on microstructure characterization, particularly for the irradiated samples.

2. Experiments

Four commercial grade ceramics were supplied by CERCOM in the USA. These ceramics were produced by vacuum hot pressing of powders, and then machined into 3 mm diameter rods. The densities of the ceramic rods were measured. Their chemical composition is listed in Table 1. Discs with a 3 mm diameter and 300 μm thicknesses were cut and then wet-polished down to a fine surface finish before irradiation.

The proton irradiation was conducted using a Tandem accelerator at the University of Wisconsin. All the samples were irradiated in the same irradiation batch with 3 discs for each ceramics, as shown in Fig. 1, along with the damage depth profiles calculated using SRIM 2003 [6]. TEM disc samples were irradiated at 800 ± 15 °C to a fluence of 2.75×10^{19} protons/cm^2, equivalent to doses of 0.71 dpa for SiC and ~1.8 dpa for ZrC and ZrN. The irradiated TEM discs were mechanically polished from the unirradiated side down to a thickness of the irradiation judging by dimple grinding to stop at roughly 30 μm from the irradiated area. Measurement of surface morphology using a profilometer indicates that the depth at which the surface fracture occurred is very close to the calculated depth where the peak damage is located.

Post-irradiation microstructural characterization was conducted at Idaho National Laboratory using a JEOL2010 transmission electron microscope operated at 200 kV. The features of the irradiated microstructure such as loops, dislocation network, cavities, and precipitates were examined. Diffraction patterns at major zone axis such as [0 1 1] or [0 0 1] were recorded for ceramics with fcc crystal structure (ZrC, ZrN). Two beam diffraction at **g** = (200) is used for bright field imaging of dislocations and loops while rel-rod dark field imaging is used to check if faulted loops were present. For the hexagonal 6H-SiC, the diffraction patterns at zone [1,−2,1,0], [0,2,−2,−1], and [0,0,0,1] are used to determine the possible lattice expansion while the diffraction of (0,0,6) or (2,−1,6) near zone [0,−1,1,0] or [1,−2,1,0] is used for the loops. The high resolution lattice fringe images for 6H-SiC basal plane projection are obtained at zone [1,−2,1,0].

The use of a higher order Laue zone (HOLZ) pattern in convergent beam electron diffraction allows a more accurate measurement of the lattice constant with an uncertainty of 0.2%. This is significantly better than the measurement using selected area diffraction (SAD) patterns [7,8]. HOLZ pattern simulation software was used to determine the lattice constant [9]. A single crystal Si sample with a known lattice constant of 0.5431 nm was used as a reference to calibrate the electron beam energy in the microscope. The HOLZ line patterns were recorded for both unirradiated and proton irradiated samples. Determination of the HOLZ patterns for the Kr ion irradiated samples from the previous work has been attempted without any success even for the 10 dpa condition due to the poor visibility of the pattern for those irradiation conditions. It is likely a result of higher radiation damage and surface oxidation at high temperature.

3. Results

The density measurement results are listed in Table 2, along with the theoretical density of these ceramics for comparison [10,11]. The higher density for ZrC (101.5% T.D.) is due to Hf (~2 wt.%) in ZrC. General features of the unirradiated microstructure for all four refractory ceramics are the uniformly distributed small defect clusters introduced by ion milling damage during sample preparation. These small defects are present even in samples ion-polished at 3 keV with an incident angle of 4 degrees. For the ceramics irradiated with protons, no voids were found in ZrC and ZrN at 1.8 dpa, and 6H-SiC at 0.71 dpa. The following sections describe the microstructure analysis for these ceramics before and after irradiation with protons at 800 °C.

3.1. ZrC

The microstructure of the unirradiated and irradiated ZrC is shown in Fig. 2. The unirradiated microstructure is dominated by a large number of small black dots due to ion milling with 5 keV Ar ions. Rel-rod dark field images did not reveal any faulted loops in the unirradiated ZrC. No precipitates were found in the unirradiated ZrC. A few scattered voids and line dislocations were found at low magnification, likely due to the fabrication process.

For the irradiated ZrC, while the bright field image at the **g** = 200 diffraction condition reveals a defect feature similar to the unirradiated condition in Fig. 2, the rel-rod weak beam dark field image shows small faulted loops with a high density at the edge-on view. The measured average size and density for the faulted loops is 7.2 nm and 4.2×10^{16} cm^{-3}, respectively. No radiation induced voids or amorphization are found in ZrC irradiated with protons at 800 °C to 1.8 dpa.

HOLZ patterns at zone [1 1 4] and the simulated matching pattern are used to measure the lattice constant for the unirradiated ZrC. The lattice constant is estimated to be 0.469 nm with 0.2% uncertainty, slightly smaller than 0.473 nm in literature [12]. The details of the HOLZ line patterns are clearly displayed in the unirradiated ZrC. There is no significant degradation on the visibility of the HOLZ pattern for ZrC irradiated with protons at 800 °C to 1.8 dpa. To evaluate the possible lattice constant change due to irradiation, a comparison of the HOLZ line pattern between the unirradiated and the irradiated ZrC is shown in Fig. 3. Both patterns look identical, indicating no lattice constant change within the uncertainty limit of 0.2%.

Table 1
Bulk composition of the refractory ceramics (wt%).

	Zr	Ti	Si	Hf	Zn	W	C	N	O	Others	Ratio*
ZrC	**84.8**	0.19	<0.001	1.91	<0.02	<0.1	**11.3**	0.61	0.21	<0.1	1.01
ZrN	**87.6**	0.095	0.007	<0.02	<0.02	0.19	0.76	**11.4**	1.43	<0.1	0.85
SiC	<0.005	<0.1	**62.08**	<0.005	<0.001	<0.05	**29.6**	0.35	0.58	Al_1.44 Fe_0.65	1.11

* The atomic ratio of the C/Zr, N/Zr and C/Si.

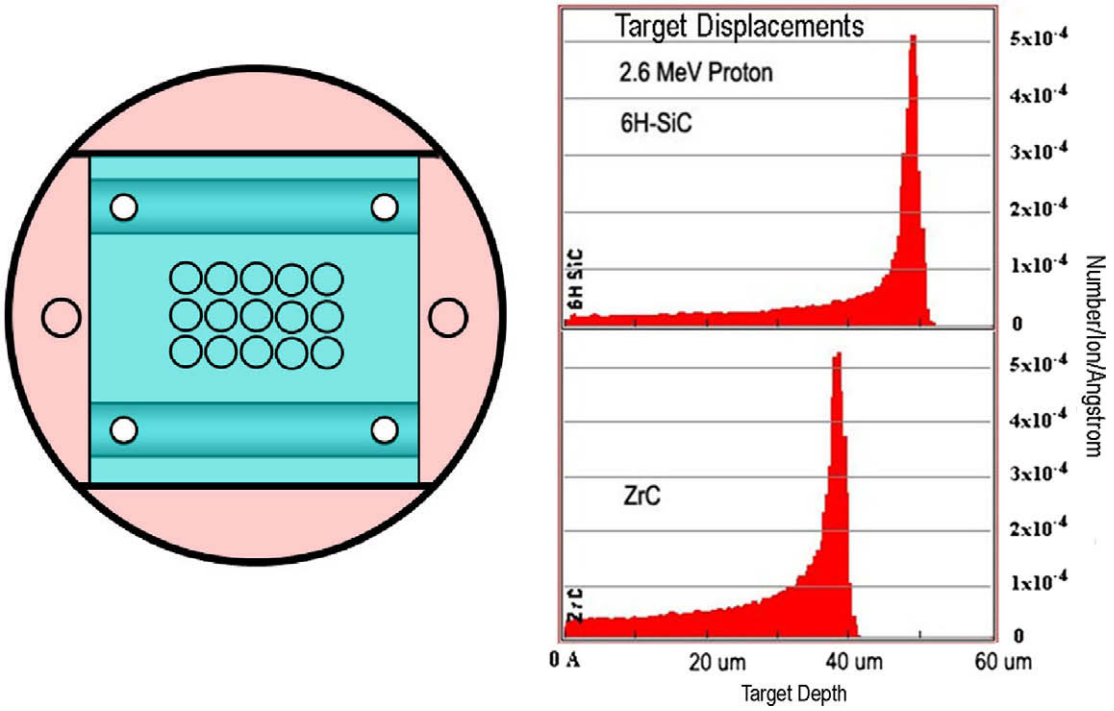

Fig. 1. Disc sample loading on the irradiation stage (left) and the calculated displacement damage profile (right).

Table 2
Density measurement for as-received ceramics (g/cm^3).

Ceramics	By dimension	By immersion	Theoretical	Immersion/Theoretical density (%)
ZrC	6.59	6.58	6.48	101.5
ZrN	7.06	7.06	7.30	96.7
SiC	3.18	3.19	3.22	99.1

3.2. ZrN

The microstructure of the unirradiated and irradiated ZrN is shown in Fig. 4. Similar to the unirradiated ZrC, the microstructure for the unirradiated ZrN reveals clear evidence of ion milling damage. There are a few areas with precipitates, scattered voids, and dislocation lines. EDS revealed circular shaped precipitates (typically < 200 nm) that are rich in Zr and O and are believed to be ZrO_2. A few large polygon shaped precipitates (typically > 1 μm) at grain boundaries are also observed. These precipitates are rich in Al and O with an atomic ratio near 2:3 and are likely Al_2O_3. The diffraction pattern and Kikuchi line pattern for the unirradiated ZrN is clear despite the defects produced by ion milling damage.

For the irradiated ZrN, the microstructure reveals no significant changes in bright field images of the defects shown in Fig. 4. The rel-rod weak beam dark field image did not show any faulted loops. The fine white spots in the rel-rod image are likely due to the black dot defects created both from irradiation and ion milling. Radiation induced voids, precipitates, and amorphization are not found in the ZrN at 1.8 dpa. No extra spots are found in the selected area diffractions.

The lattice constant for the unirradiated ZrN is measured to be 0.458 nm using a HOLZ line pattern from the best match to the simulated pattern, consistent with the literature data of 0.4575 nm [9]. A comparison of HOLZ patterns between the unirradiated and the irradiated ZrN is shown in Fig. 5. Similar to ZrC, there is no discernable change between the unirradiated and the irradiated patterns. The lattice constant change due to irradiation is believed to be within the uncertainty limit of 0.2%.

3.3. SiC

For the hexagonal SiC there are many possible configurations due to the variation in its stacking sequence along the [0001] crystal direction. The SiC used in this work is a 6H-SiC. The stacking sequence repeats after every 6 layers of Si along [0001]. For the unirradiated SiC, the microstructure is summarized in Fig. 6. Most of the areas on the sample show uniform matrix with little evidence of ion milling damage from sample preparation in contrast to the unirradiated ZrC and ZrN. The microstructure is decorated with scattered dislocations and significant amount of stacking faults (see Fig. 6, top set of pictures). Due to the large lattice constant (c = 1.5117 nm), the projection of the basal planes at edge-on condition is clearly visible by imaging at zone [1,−2,1,0] without using the objective aperture (see Fig. 6, bottom set of pictures). A close look at stacking faults reveals the spacing variation between the fringes due to stacking faults on basal plane.

For SiC irradiated with protons at 800 °C to 0.71 dpa, irradiation induced defects in comparison with that of the unirradiated SiC are shown in Fig. 7. The bright field image with $\mathbf{g} = (006)$ shows small black dot defects at high density in the irradiated sample. The high resolution view of the basal plane projection at magnification of 100 K and 400 K also reveals a significant increase in the number of defects in the irradiated SiC. Similar to the unirradiated case, stacking faults are still present as a main microstructure feature in the 0.71 dpa SiC. There is no noticeable degradation in the visibility of Kikuchi patterns in convergent beam diffraction for the irradiated SiC.

To evaluate if there is any lattice constant change due to irradiation, a comparison of the high resolution images for basal plane projection is shown in Fig. 8. The match on the two sets of fringes between the unirradiated and the irradiated SiC indicates no change on the basal plane spacing, therefore no lattice constant

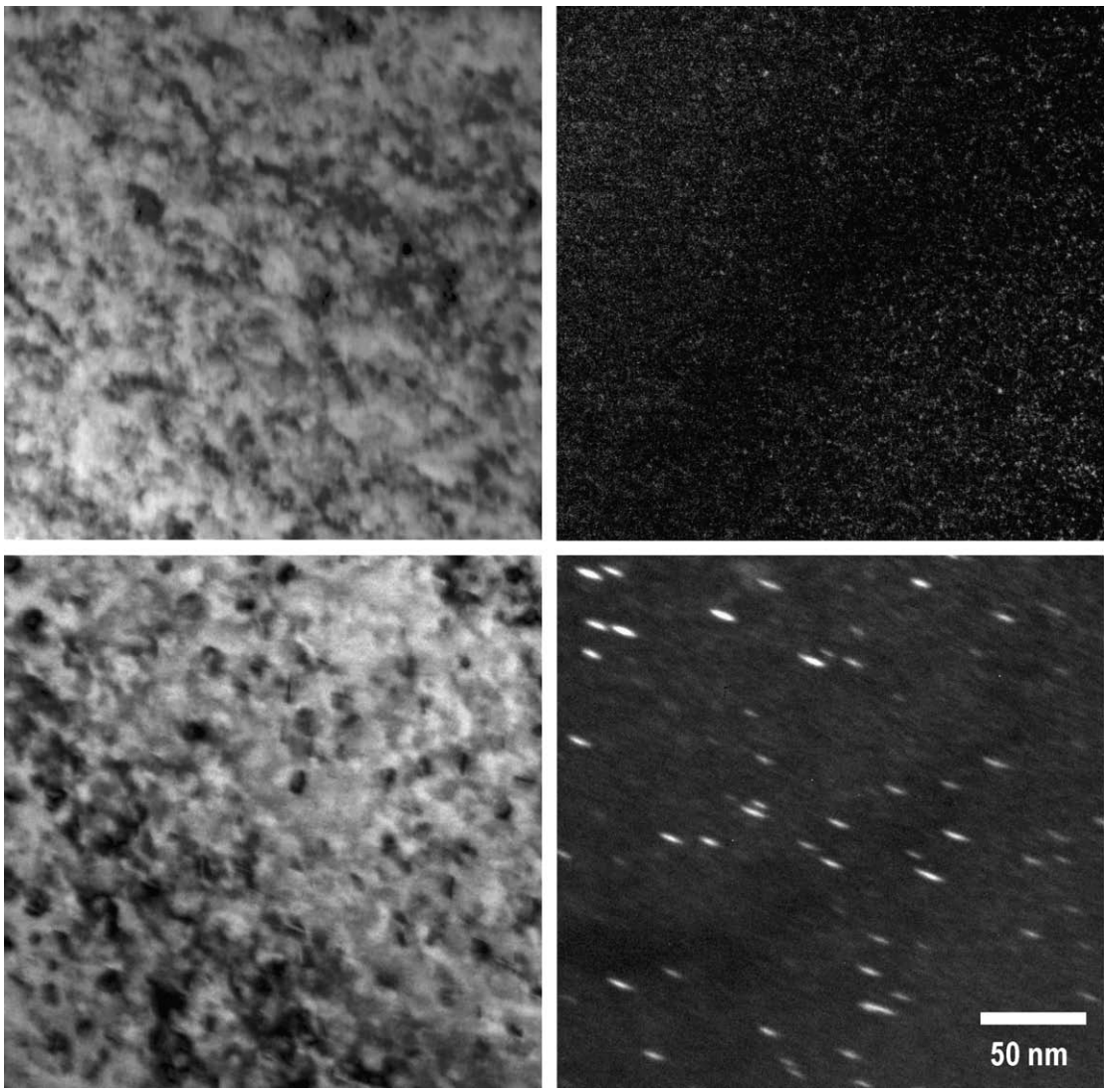

Fig. 2. Microstructure of the unirradiated ZrC (top) and the irradiated ZrC (bottom) imaged with **g** = 200 near zone [011] (left) showing black dot damage from ion milling and the rel-rod weak beam dark field image (right) showing faulted loops only in the proton irradiated ZrC (800 °C to 3.0 dpa).

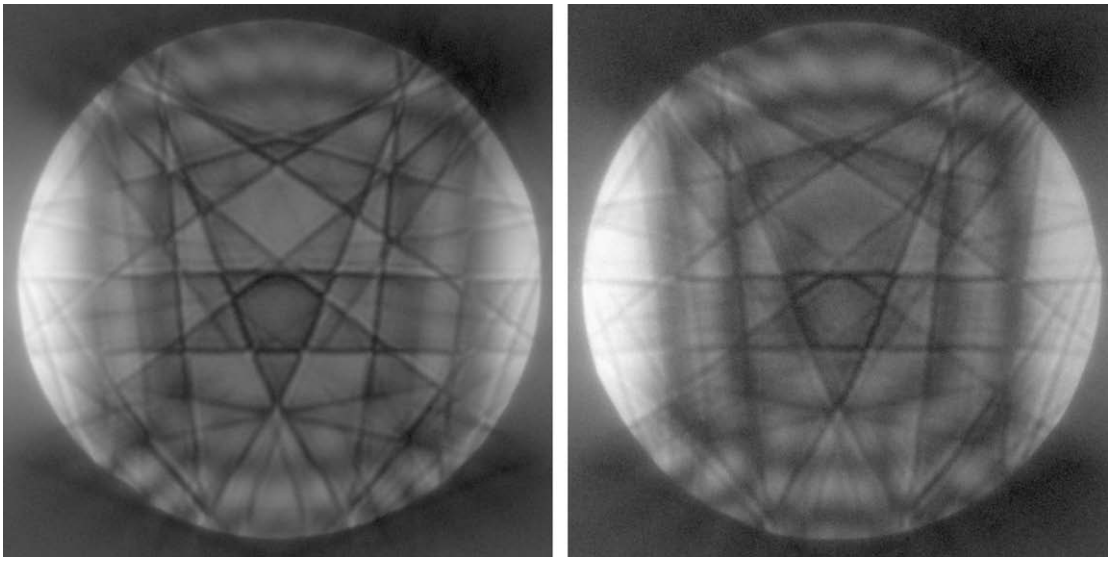

Fig. 3. Comparison of HOLZ patterns at zone [114] for the unirradiated ZrC (left) and irradiated ZrC (right) with protons at 800 °C to 3.0 dpa, showing no noticeable change in lattice constant.

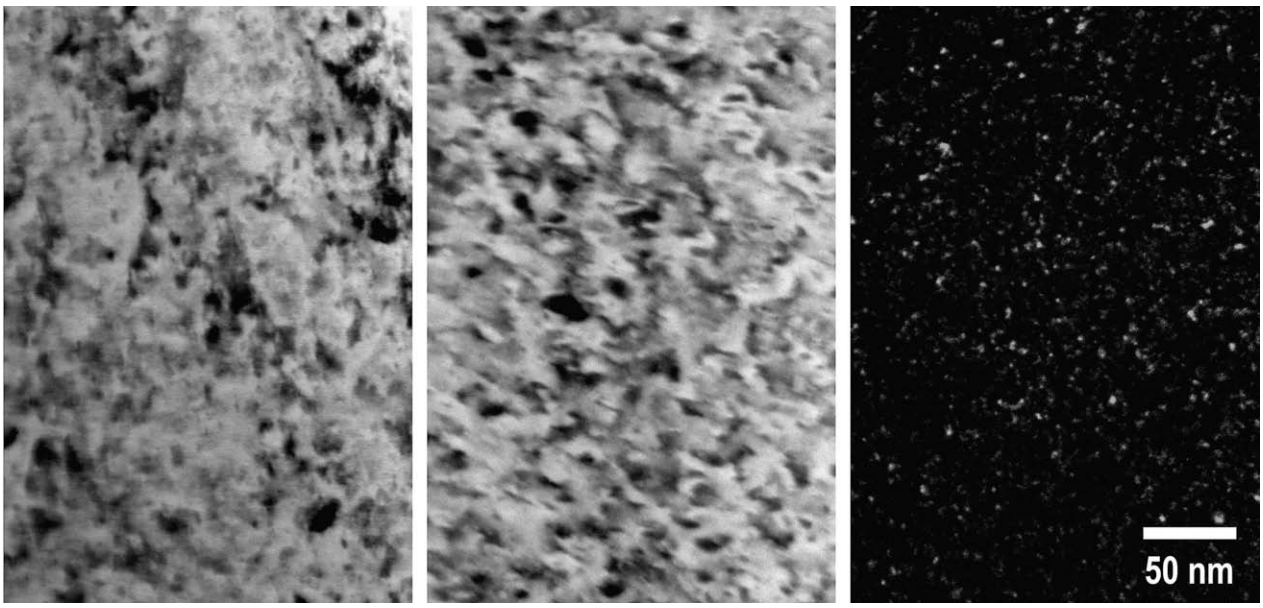

Fig. 4. Microstructure of unirradiated ZrN (left) and the irradiated ZrN (middle) imaged with **g** = 200 near zone [011]. Faulted loops are not found in the rel-rod weak beam dark field image in the ZrN irradiated with protons at 800 °C to 3.0 dpa (right).

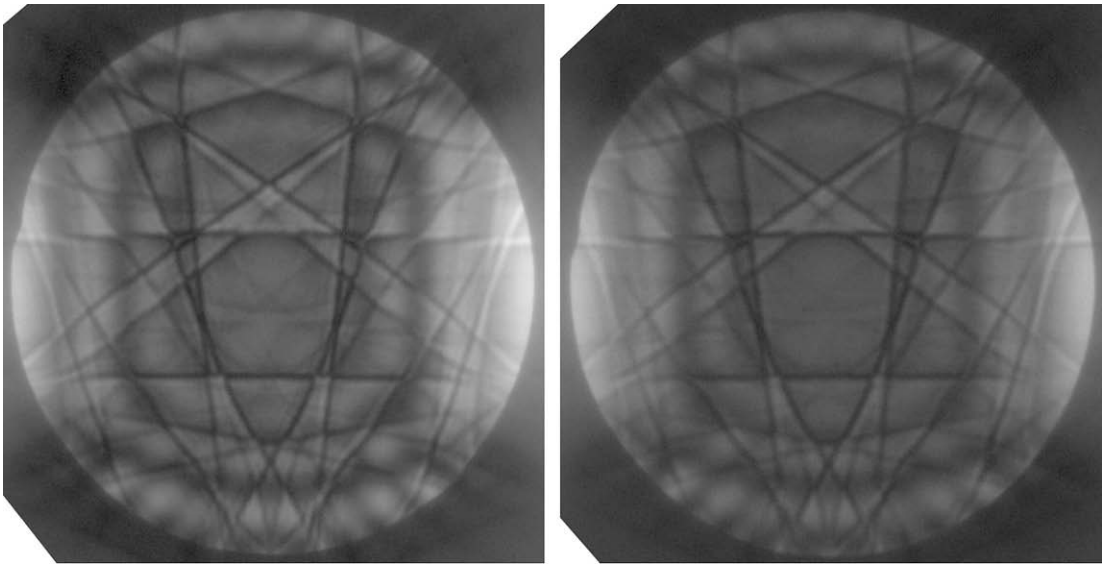

Fig. 5. Comparison of HOLZ patterns at zone [1 1 4] for the unirradiated ZrN (left) and irradiated ZrN (right) (800 °C to 3 dpa), showing no noticeable change in lattice constant.

change in *c*. The experimental HOLZ line patterns at zone [0 0 0 1] for the unirradiated and the irradiated 6H-SiC are presented in Fig. 9. The difference in the polygon fringes is due to the difference in the thickness where the HOLZ line pattern was recorded. There is no discernable difference in the HOLZ line patterns between the two conditions, indicating no lattice constant change in a.

4. Discussion

The discussion of the results of the proton irradiation (2.6 MeV, 800 °C) will be contrasted with the results from previous work using Kr irradiation (1 MeV, 800 °C) on the same batch of ceramics. Note that there is a large difference ($\sim 10^3$) in displacement damage rate between Kr ion and proton irradiation. It is worth mentioning that proton irradiation provides a displacement damage rate similar to the GFR core ($\sim 10^{-6}$ dpa/s) with reasonable irradiated volume (depth $\sim$30 μm), but is limited by its practically achievable dose ($\sim$10 dpa), while Kr ion irradiation has an advantage to achieve very high dose ($\sim 10^2$ dpa), but is limited by the very small irradiated volume (depth < 1 μm). Proton irradiation creates an irradiated microstructure representing bulk microstructural change. TEM sample preparation after proton irradiation prevents any surface effects on the microstructure from irradiation. This is a great advantage over the Kr irradiation where the thin area of a TEM sample is irradiated in-situ in an intermediate voltage electron microscope equipped with an accelerator.

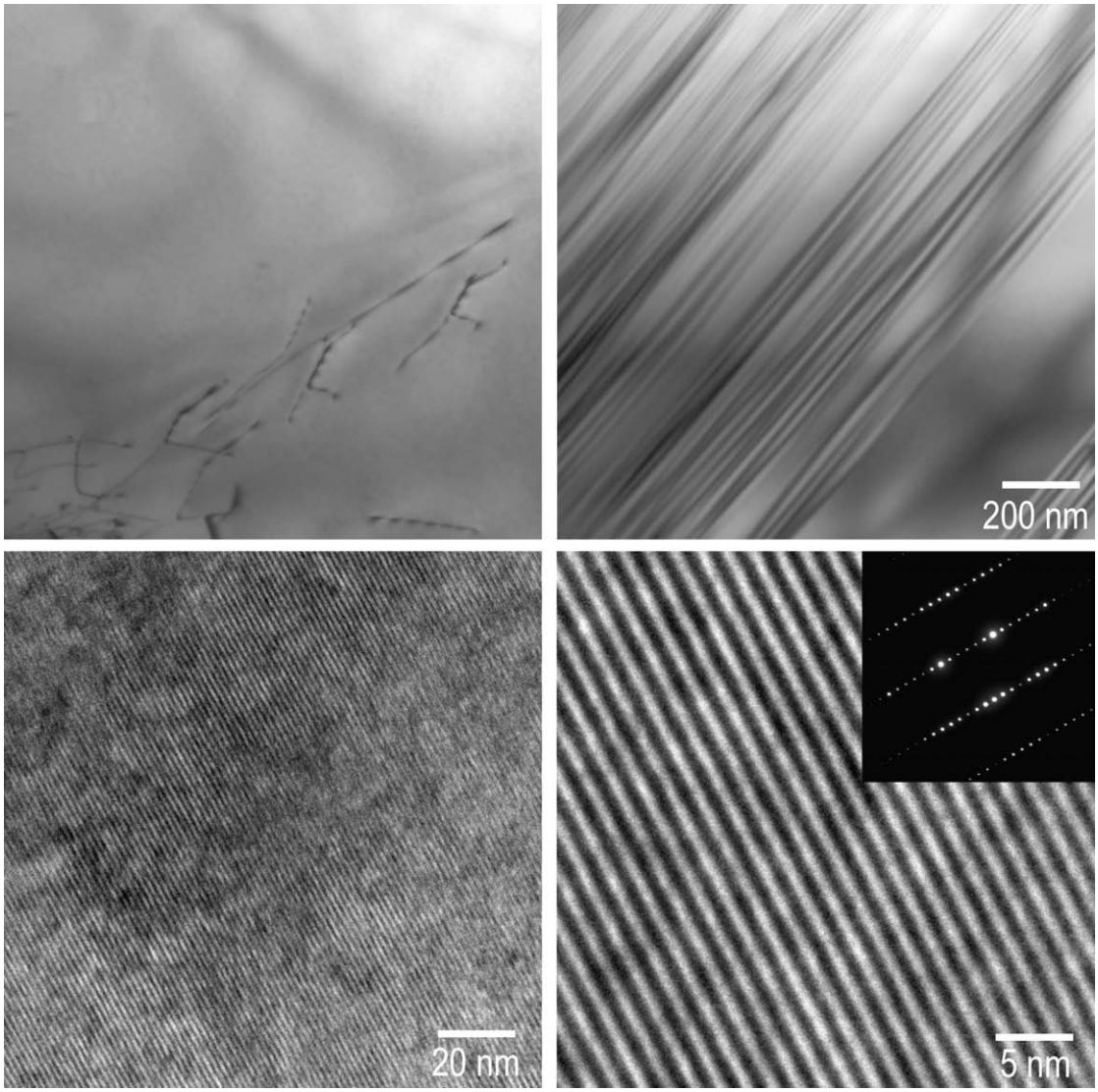

Fig. 6. Microstructure of the unirradiated 6H-SiC. It shows scattered dislocations (top-left) and a group of stacking faults (top-right). The high resolution images (bottom) reveal the projection of basal planes at edge-on condition. The insert shows the diffraction at zone [hkil] = [1,−2,1,0] which is used to form the high resolution images.

4.1. ZrC

The faulted loops on the (1 1 1) planes are typical defect features in irradiated fcc metals. These loops are effective barriers to mobile dislocations and contribute significantly to radiation hardening in the materials. The small sizes and high density of these loops in ZrC irradiated at 800 °C are likely due to the relative low irradiation temperature compared to its melting point (T_{irr}/T_m = 0.28) [10]. The previous Kr ion irradiation at 800 °C to both 10 and 70 dpa did not reveal faulted loops. It was thought the crystal structure in ZrC (two sets of fcc structures overlapping) was responsible for the lack of faulted loops. Knowing the difference of three orders of magnitude in displacement damage rate, proton irradiation seems more effective in producing faulted loops for the given irradiation temperature. This is possibly due to the kinetics for interaction and migration of point defects and defect clusters in favor of faulted loop formation. Unlike the Kr ion irradiated ZrC, a ring pattern in the selected area diffraction is not observed in the proton irradiated sample. It is realized that the previous microstructure analysis for Kr ion irradiation at 800 °C is complicated by the surface problems such as oxidation. It suggests less surface effect on proton irradiated samples compared to Kr ion irradiation at high temperature.

Although small bubbles existed in the unirradiated sample from ion milling with Ar ions, the lack of void development in the proton irradiated ZrC may be attributed to both the low irradiation temperature and crystal structure for ZrC. In fcc metals, void formation typically occur in an intermediate temperature range (T_{irr}/T_m = 1/3–1/2). The result of the proton irradiation is consistent with Kr ion irradiation where no voids were found even at doses up to 70 dpa. Unlike the fcc metals, the crystal structure of ZrC can be envisioned as a fcc lattice of Zr with *c* filling in the octahedral interstitial sites. Irradiation produces point defects and defect clusters in the material. The evolution of these defects and clusters under radiation-enhanced diffusion, plus the interactions of these defects with various sinks, determines the irradiated microstructure. According to the work by Li [13] on the inter atomic potential of ZrC, the properties of ZrC are dominated by the strong covalent bonds and the weak ionic bonds (Zr–C), and the original metallic bonds (Zr–Zr) can be neglected. It is possible that this unique structure and strong chemical bonding may significantly slow down the diffusion and increase the formation energy for both voids and faulted loops. Radiation induced amorphization is not identified in either the proton or Kr ion irradiations at 800 °C, indicating the crystal

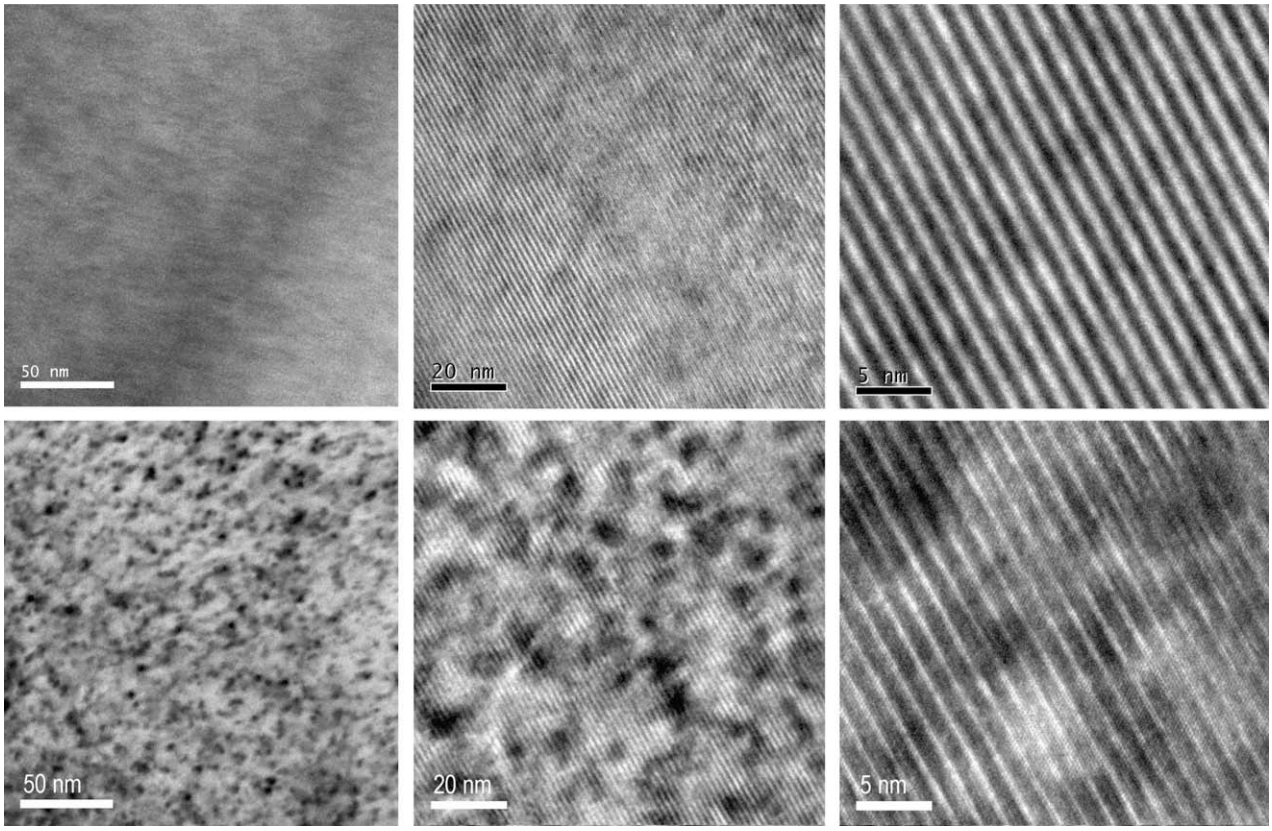

Fig. 7. Comparison of microstructure for the unirradiated (top) and proton irradiated (bottom, 1.5 dpa) 6H-SiC in bright field images with **g** = 006 (left) and high resolution images at zone [1,−2,1,0] showing defects and projection of basal planes (middle and right).

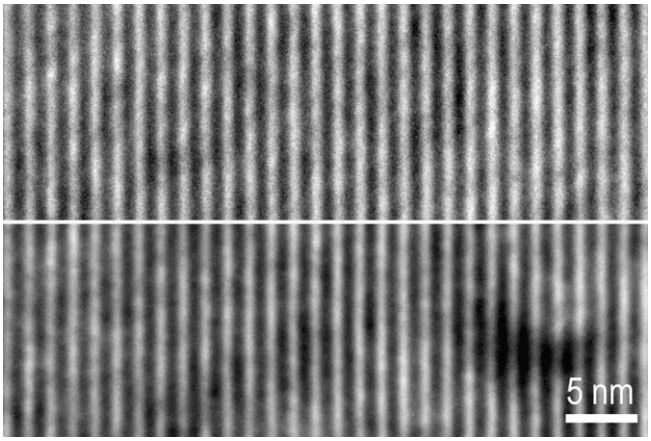

Fig. 8. Comparison of high resolution images of basal plane projection between the unirradiated (top) and irradiated 6H-SiC (bottom) at zone [1,−2,1,0], showing no change in basal plane spacing from proton irradiation at 800 °C to 1.5 dpa.

structure is stable against amorphization at the given irradiation temperature.

The visibility of the Kikuchi pattern and HOLZ line pattern in convergent beam electron diffraction may be used to qualitatively evaluate the crystal structure integrity. It seems the latter is more sensitive to the distortion on the crystal atomic planes in the lattice. In proton irradiated ZrC (1.8 dpa), there is no noticeable degradation on the visibility of both Kikuchi pattern and HOLZ line pattern. This is in contrast to Kr ion irradiation where the visibility of Kikuchi pattern degrades noticeably at 10 dpa and severely at 70 dpa while the visibility of the HOLZ line pattern already drops to zero at 10 dpa. These comparisons suggest that the crystal atomic plane suffers less distortion from irradiation with protons to 1.8 dpa than with Kr ions to 10 dpa. This allows the use of HOLZ patterns to measure the lattice constant and its changes in the proton irradiation case with significantly less uncertainty (0.2%) when compared to the use of SAD patterns. Measurements of lattice constants using SAD patterns may carry an uncertainty greater than 1%, likely due to the difficulty in sample height control in the TEM even with good alignment and calibration [6,7].

The measured lattice constant is slightly smaller than the literature data, possibly due to the presence of 2% Hf in the material. Comparison of the HOLZ line patterns between the unirradiated and the irradiated condition shows no noticeable difference, indicating a lattice constant change less than 0.2%. This result is inconsistent with neutron irradiated ZrC at 130–355 °C to 7.5 dpa where a 2.5% volume increase is observed and believed mostly caused by the defect clusters [1]. Unfortunately, there is no microstructural analysis for their work. It is anticipated that neutron irradiation to 7.5 dpa will produce more damage to microstructure than proton irradiation to 1.8 dpa at comparable temperature. The large difference in the irradiation temperature between proton and neutron data makes the comparison difficult and it is hard to draw any meaningful conclusion. This is a typical case for radiation study on GFR ceramics since the reference data on radiation performance for these candidate ceramics under irradiation conditions relevant to GFR cores does not exist.

4.2. ZrN

The major difference between the proton irradiated ZrC and ZrN is the lack of faulted loops in ZrN. The Kr ion irradiation also reveals large difference in microstructural response to irradiation between

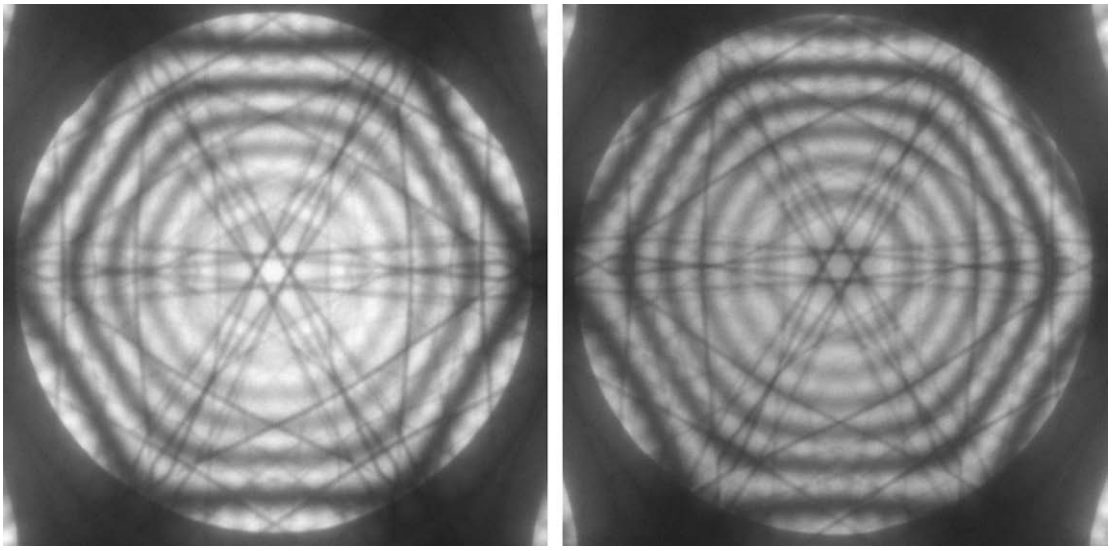

Fig. 9. Comparison of HOLZ line patterns at zone [0 0 0 1] between the unirradiated (left) and the irradiated 6H-SiC (right, 1.5 dpa at 800 °C), showing no change in lattice constant.

ZrC and ZrN in a different aspect. It suggests that carbides and nitrides act significantly differently in the microstructure evolution under irradiation. The exact cause for the lack of faulted loops in ZrN is not clear. One obvious explanation is that nucleation of faulted loops is more difficult in ZrN than in ZrC. Similar to ZrC, no radiation induced amorphization or precipitation is observed in the proton irradiated ZrN.

While Moire fringes and ordered fcc structure developed as major features in Kr ion irradiated ZrN, none of these features are found in the proton irradiated ZrN. Like ZrC, the visibility for the Kikuchi pattern and the HOLZ line pattern under convergent beam electron diffraction for proton irradiated ZrN shows no discernable degradation. For Kr ion irradiated ZrN at 10 dpa, the visibility for the HOLZ line pattern drops to zero and the visibility for Kikuchi patterns degrades. The comparison indicates proton irradiation to 1.8 dpa causes less distortion on the lattice than Kr irradiation to 10 dpa for ZrN, consistent with proton irradiated ZrC. It is believed that the surface oxidation developed in Kr ion irradiated ZrN may be partially responsible for its complex microstructural development.

The lattice constant (a = 0.458 nm) measured using the HOLZ line pattern at zone [1 1 4] is in excellent agreement with the literature data (a = 0.4575 nm). The comparison of the HOLZ patterns between the unirradiated and the irradiated ZrN shows no noticeable changes in line pattern. This indicates the change in lattice constant due to proton irradiation is less than 0.2%. Similar to ZrC, no compatible case for neutron irradiation can be found in the open literature for a meaningful comparison.

4.3. SiC

In the following discussion, SiC refers to 6H-SiC unless otherwise specified. The difference in the unirradiated microstructure between SiC and the other ceramics is obvious by comparison in Figs. 2, 4 and 6. The microstructure characterization for the unirradiated SiC suggests that SiC has the least radiation damage from ion milling among the five ceramics. SiC have the largest unit volume (0.1242 nm^3), lowest molecular weight (40.1), and the smallest atomic size for Si comparing to Ti and Zr. These differences may be partially responsible for its good resistance to the ion milling damage during sample preparation. The scattered dislocations in the unirradiated SiC are likely from materials fabrication. The high density of stacking faults in 6H-SiC is a common feature in microstructure for this material. Although some details of the basal planes are revealed by the high resolution image at zone [1,−2,1,0], as shown in Fig. 6, a true high resolution image with much more detail on atomic arrangement can only be obtained by using a dedicated high resolution TEM microscope.

The comparison of the microstructure between the unirradiated and the irradiated SiC (0.71 dpa) reveals the presence of black dot type defects at high density, as shown in Fig. 7. The chemical and crystal structure analysis for these small defects was not successful due to their small size. Some of these small defect features may be loop embryos. But no well defined loops can be identified. In the Kr ion irradiation, well defined loops are only exhibited in SiC irradiated to 70 dpa. According to Persson's work [4], these loops are most likely interstitial loops residing on (0 0 0 1) planes. Since loops only developed at very high dose in Kr irradiated SiC, the dose for proton irradiation to 0.71 dpa may be too low to see the loops. Considering the well defined defect features in proton irradiation at 0.71 dpa in contrast to relatively clean microstructure after Kr irradiation at 10 dpa, the difference in microstructural development between these two irradiations is demonstrated.

The lattice constant change from proton irradiation is examined using both high resolution images of basal plane projection and the HOLZ patterns. The comparison of the fringe spacing from high resolution images of basal plane projection indicates no change from proton irradiation in the lattice constant, c, as shown in Fig. 8. The HOLZ line patterns look identical between the unirradiated and the proton irradiated SiC, suggesting the change in lattice constant, a, is less than 0.2%. This is consistent with the results from Kr ion irradiation where lattice constant change was not seen even at 70 dpa using selected area diffraction pattern. Proton irradiation to 0.71 dpa for SiC shows no effect on the visibility of both the Kikuchi pattern and the HOLZ pattern.

5. Conclusion

Proton irradiation at 800 °C to 1.8 dpa in ZrC produced small faulted loops at high density. No loops are found in ZrN irradiated under the same condition. The HOLZ line patterns are clearly visible in ZrC and ZrN irradiated with protons to 1.8 dpa, but not in the same ceramics irradiated with Kr ions to 10 dpa. This may be attributed to the lower dose achieved in the proton irradiation

for these ceramics. Proton irradiation produced uniformly distributed black dot type defects in SiC at 0.71 dpa, in contrast to Kr ion irradiation where no visible radiation induced defect features were observed at 10 dpa. The well defined defect features in proton irradiated ZrC and SiC suggests that protons are more effective at producing radiation damage in microstructure than Kr ions at 800 °C. Unlike the complex microstructural response obtained with Kr irradiation in previous work, the irradiated microstructure in proton irradiation is relatively simple, possibly due to the lower dose and the benefit of eliminating the adverse surface problem.

The use of HOLZ line patterns in proton irradiated ceramics allows accurate determination of the lattice constant and its changes in the three ceramics investigated. The comparison with HOLZ line patterns between the unirradiated and the irradiated ceramics indicates no change in lattice constant within an uncertainty limit of 0.2%. While 6H-SiC was identified as the best ceramics based on the microstructural stability under Kr irradiation among the five ceramics in previous work, the same conclusion cannot be made in this proton irradiation study, possibly due to the relatively low dose. In this work, ZrN shows less microstructural change to proton irradiation as compared to ZrC and SiC.

Acknowledgements

The authors would like to express their gratitude to Brandon Miller, Hannah Yount, and Kim Kriewaldt at the University of Wisconsin Ion Beam Laboratory for their assistance with the proton irradiation. This work was supported through funding provided by the US Department of Energy (DOE) to the Generation IV program on GFR Materials at the Idaho National Laboratory, operated by Battelle Energy Alliance, LLC, under DOE Idaho Operations Office Contract DE-AC07–05ID14517.

References

[1] D.A. Dyslin, R.E. Moore, H.E. Robertson, ORNL-4480 (1969) 245.
[2] W.J. Weber, L.M. Wang, N. Yu, Nucl. Instrum. and Meth. B 116 (1996) 322.
[3] P.O.A. Persson, L. Hultman, M.S. Janson, A. Hallen, R. Yakimova, J. Appl. Phys. 93 (5) (2003) 9395.
[4] P.O.A. Persson, L. Hultman, M.S. Janson, A. Hallen, R. Yakimova, D. Panknin, W. Skorupa, J. Appl. Phys. 92 (5) (2002) 2501.
[5] FY-2005 Summary Report: Ion Irradiation Study on Microstructure Stability of GFR Ceramics: ZrC, ZrN, TiC, TiN and SiC Irradiated with 1 MeV Kr-Ions to 10 and 70 dpa at 800 °C. <https://inlportal.inl.gov/portal/server.pt/gateway/PTARGS_0_200_3310_277_2604_43/http%3B/inlpublisher%3B7087/published-content/publish/communities/inl_gov/about_inl/gen_iv___technical_documents/gfr_ceramics_ion_irradiation.pdf>, 2005.
[6] J.F. Ziegler, J.P. Biersack, U. Littmark, The Stopping and Range of Ions in Solid, Pergamon, New York, 1996.
[7] D.B. Williams, C.B. Carter, Transmission Electron Microscopy, Plenum, New York and London, 1996.
[8] J.C.H. Spence, J.M. Zuo, Electron Microdiffraction, Plenum, New York and London, 1992.
[9] X.Z. Li, J. Appl. Crystallogr. 38 (2005) 576.
[10] W. Lengauer, S. Binder, K. Aigner, P. Ettmayer, A. Guillou, J. Debuigne, G. Groboth, J. Alloys Compds. 217 (1995) 137.
[11] K. Aigner, W. Lengauer, D. Rafaja, P. Ettmayer, J. Alloys Compds. 215 (1994) 121.
[12] T.B. Massalaski, H. Okamoto, P.R. Subramanian, L. Kacprzak, (Eds.), Binary Alloy Phase Diagrams, 2nd Ed., ASM International, 1990.
[13] J. Li, J. Appl. Phys. 93 (11) (2003) 9072.